# Anatomical and mechanical properties of the tympanic membrane

W.F. Decraemer[1] and W.R.J. Funnell[2]

[1]*Department of Biomedical Physics, University of Antwerp, Antwerpen, Belgium;*
[2]*Departments of BioMedical Engineering & Otolaryngology, McGill University, Montréal, Canada*

## Introduction

The middle ear is a small, complex three-dimensional (3-D) mechanical system that serves the physical function of collecting acoustical energy from a sound wave in air and passing it to the microscopic electro-mechanical sensory system of the inner ear. The system works over a very broad frequency range, has a large dynamic range and is able to function under greatly different static pressure conditions. The middle ear is too complex a system for its function to be understood intuitively; good numerical parameter values for inclusion in accurate mathematical models are therefore very much required.

Essentially, 1-D mathematical models such as lumped circuit models are valuable, but often limited due to the simplifications involved in their definition. For example, representing a tympanic membrane (TM) as a combination of a few mass, stiffness and damping elements cannot account for the complex vibration patterns at higher frequencies. Similarly, the ossicles cannot be modelled as a solid block pivoting about a fixed rotational axis and having a fixed moment of inertia. For many purposes all structural elements – the TM and the ossicles and their links to the middle-ear cavity walls – must all be modelled with precision, and distributed 3-D models should be used. Accurate values of all physical parameters concerned are required. Some properties such as TM shape, thickness and elasticity are of major importance for TM function. This review will emphasize studies of these three parameters that have been performed over the last three decades.

In this chapter we shall consider the anatomical properties of the human TM and the TMs of two of the most common animal models in hearing research, cat and gerbil. Before discussing recent observations on some of the crucial an-

atomical and mechanical properties of the TM, we let ourselves be guided by the review of Funnell and Laszlo[1] in drawing the state of the art of observations on TM structure in various species around 1980. Along the way, we shall mention where major advances have been made between 1980 and 2007, the present review period. First, we will briefly discuss the structure of the TM. In the following sections we will then discuss TM shape, thickness and material properties, respectively, in each case starting with a summary as of the early 1980's and then discussing more recent observations.

## Tympanic membrane structure

The typical mammalian TM consists of a *pars tensa* and a smaller *pars flaccida*. The pars tensa is a tri-laminar membrane, with an inner mucosal layer, an outer epidermal layer and an intermediate fibrous layer. The annular ligament firmly anchors the pars tensa to the bone of the tympanic ring around most of its circumference, and the manubrium of the malleus is more or less tightly coupled to it. The outline of the pars tensa varies across species, from approximately circular to a more or less elongated ellipse. The manubrium may be placed symmetrically, or it may be somewhat closer to the antero-superior edge of the pars tensa. It may be approximately perpendicular to the nominal axis of ossicular rotation (from the anterior mallear process to the posterior incudal process) or it may be very oblique. Figure 1 shows outlines of the TMs of a number of mammalian species, all drawn to approximately the same scale. In each case the outline is oriented so that the nominal rotation axis is approximately horizontal. It is worth noting that the orientation of the manubrium was recently found to be remarkably variable in humans.[2]

The pars flaccida is a smaller part of the TM, superior to the manubrium that differs anatomically and functionally from the pars tensa. The size of the pars flaccida is very variable, as seen in Figure 1: it is very large in the sheep, mouse and gerbil, and absent in the guinea pig. In man and cat it is moderately small. Knowledge about the role and function of the pars flaccida under acoustical and static pressure loads was extended in the present review period. Teoh *et al.*[3] showed that the large pars flaccida in the gerbil reduces the sensitivity at low frequencies. Dirckx *et al.*[4] showed that in gerbil the pars flaccida flips from its outermost lateral position to its innermost medial position within a very small range (± 200 Pa or about 20 mm $H_2O$) of static pressures. The total pars flaccida volume displacement Dirckx *et al.* measured was found to be too small to provide for the often-presumed protective mechanism against large static pressures [*e.g.,* 5]. It has been hypothesized [6] that this great pressure sensitivity of the pars flaccida may be indicative of a role for it as a detector for small static middle-ear pressures, possibly involved in the opening and closing of the Eustachian tube.
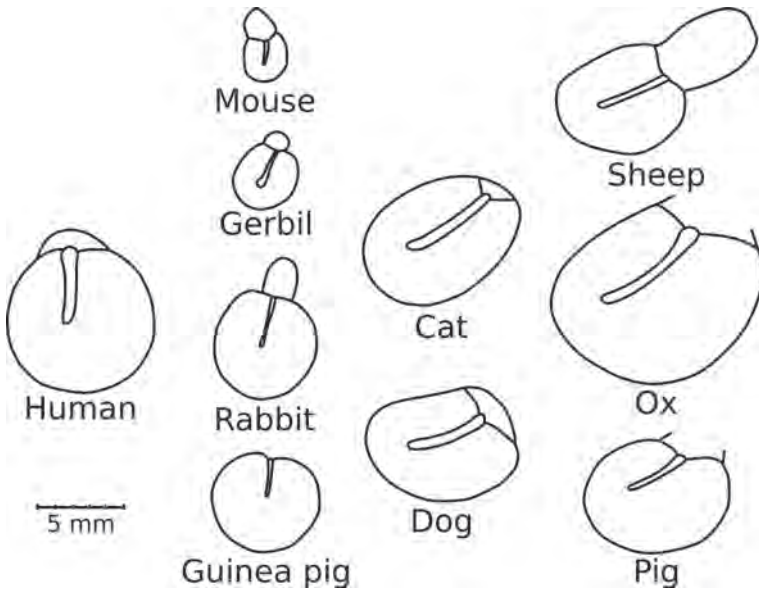
*Fig. 1.* Outlines of the TMs of a number of mammalian species, all drawn to approximately the same scale. Two features may immediately be noted as being very variable: the size of the pars flaccida and the angle between the manubrium and the nominal rotation axis. Note that the TMs shown are all of similar size in spite of the great body-size differences among the species. (Mouse after Reijnen & Kuijpers, 1971; cat after Khanna, 1970; gerbil based on our micro-CT scans; sheep after Lim, 1968b; all others after Fumagalli, 1949)

## Tympanic membrane shape

The TM, and in particular the pars tensa, can be described as a cone with curved sides. In this section we briefly review measurements of the overall conical shape and of the curvature as of about 1980, and then present more recent data.

### Conical shape

The typical mammalian TM is approximately conical, with the apex pointing medially. In a 1949 study, Fumagalli[7] found that the TM shapes of all nine species that he observed could be represented approximately by a cone with an apex angle of 120°, cut at various angles by the plane of the tympanic ring. The angle was correlated with the obliqueness of the manubrium mentioned in the previous section, with the guinea-pig TM, *e.g.,* being a right cone.

### Curvature

The sides of the cone formed by the TM are convex outward. This seems to be universal among terrestrial mammalian TMs.

Around 1980, there were no reliable and precise data in the literature concerning the actual curvature of the TM. Kojo in 1954[8] and Kirikae in 1960[9] had studied paraffin castings of the human TM, but their published accounts are sketchy and their data were probably distorted by the casting process. Kirikae also measured the angle included in the apex of the curved cone formed by the TM in each of several species, but reported only that it 'ranged from 97° for Barbary sheep to 135° for the mole and squirrel in mammals'. He noted that the ungulates and carnivora had relatively small apex angles and generally had long manubria (compared with the diameter of the TM) while other animals, with larger apex angles, had short manubria with the umbo located near the centre of the TM.

Khanna & Tonndorf[10,11] introduced moiré topography, an optical technique, to study the three-dimensional shape of the cat TM using a refined casting technique. Funnell[12] provided image-processing techniques for interactive analysis of the resulting interferometric fringe maps. These attempts were hampered by poor resolution and uncertain boundary definition.

Since then, a sophisticated automated phase-shift shadow-moiré technique was developed and used for precise full-field shape measurements of TMs of human, cat and gerbil (see below).

## New observations on tympanic membrane shape

As mentioned above, it is important in mathematical modelling to include a natural TM shape. Recently we have advocated that, for the analysis and communication of experimental results on TM vibrations, the knowledge of the 3-D geometry of the structure measured is very important.[13] When measuring TM vibration, for example, one has not only to specify the measurement location but also the angle that the measured component makes with the surface normal and/or the annulus plane, so that results from different experiments can be meaningfully compared.

As with most anatomical features, the size and shape of the TM are highly variable from one individual to another. Comparing experimental data from a given experiment with calculations based on a standard ear model is often unrewarding. It may therefore be more important here to present techniques for measuring TM shape than to discuss general features of the TM. In the next section we start by describing some shape-measurement techniques and end with some measurement examples.

*Shape-measurement tools*

Moiré topography

To measure the shapes of delicate surfaces such as TMs, we designed in the laboratory in Antwerp successive versions of non-contacting, full-field measuring devices based on moiré interferometry.[14,15-21] A shadow of a grating of parallel lines is cast onto the TM, which must be coated with, for example, a thin layer of white drawing ink or magnesium oxide to make the TM diffusely reflective. The grating image on the TM is modulated by the TM topography, and the moiré interference between it and the undistorted line grating results in a pattern of moiré fringes that overlays the image of the TM as a set of equi-distant height contours. The fringe interval can be determined by using a calibration object such as a cylindrical cone. Using fringe patterns with intermediate known fringe shifts, we can calculate a shape matrix with the column and row numbers proportional to the $x$ and $y$ coordinates, respectively, and with the depth information $z(x,y)$ stored as matrix element. This matrix can be shown as a shape image with, for example, the pixel grey level proportional to depth. An example image from a human TM study[22] is shown in Figure 2a, with the annulus and the edge between pars tensa and pars flaccida outlined. The same data can also be shown as a 3-D plot, as shown in Figure 2b.

To apply the technique for TM measurements, the surface of the TM has to be made freely visible over an angle of about 10 to 30° (one of the factors de-
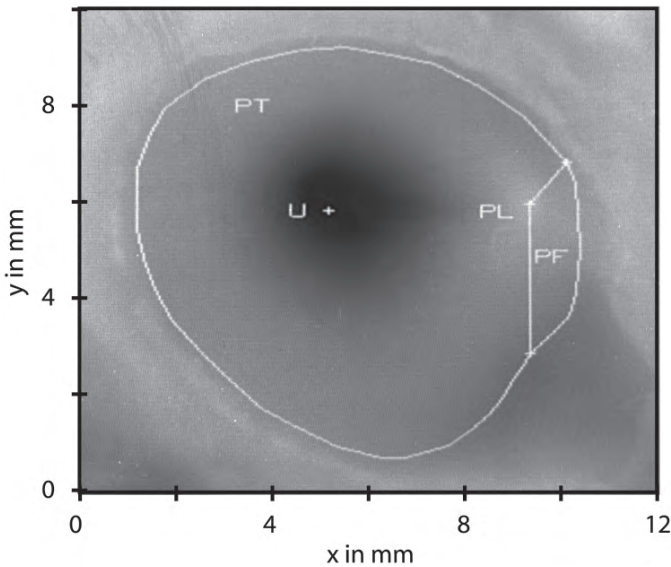


*Fig. 2.* (a) A grey-level shape image of a human TM, obtained by attributing to each pixel with coordinates $(x,y)$ a grey level proportional to the local depth $z(x,y)$. Some landmarks are annotated.
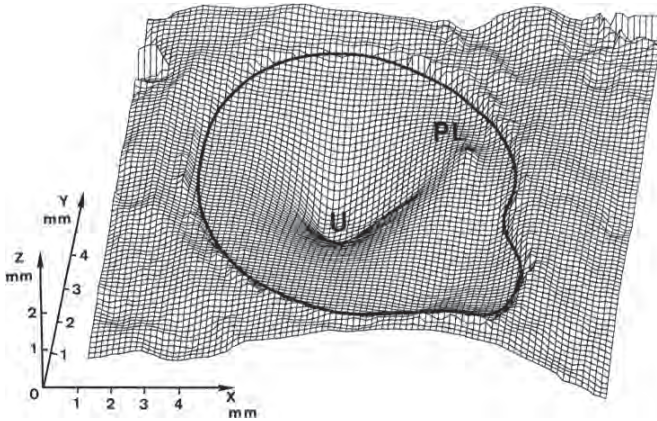
*Fig. 2.* (b) The shape matrix $z(x,y)$ from (a) is here shown as a 3-D surface. Parts outside the annulus represent the trimmed bone and can be disregarded.

fining resolution). For measurements in human and cat the lateral TM surface was observed after cutting down the ear canal as far as possible without damaging the annulus. Some remaining bone overhanging the TM edge in the inferior region cannot be avoided. For many purposes this can be neglected.

By recording images for a set of static under- and overpressures applied to the middle ear cavity, the functional circumferential border of the TM (where the TM displacements under either static or dynamic pressure load are zero) can be determined.[23] Using moiré maps obtained under different static pressure loads is especially helpful in determining the functional border of the TM in the superior region where the epithelium on the TM surface continues without visual demarcation or change in slope onto the superior bony wall of the ear canal, and, using extrapolation, in regions with significant overhanging bone. Figure 3 shows a cat TM with functional borders at the manubrium and annulus, and between the pars tensa and pars flaccida, determined with the aid of shape images for different pressures.

For gerbil TM measurements, we exposed the medial surface after dissecting away the incus, stapes and cochlea, and there was no problem of overhanging bone. A few drops of diluted white drawing ink in the ear canal formed a thin liquid layer on the TM; the TM in the gerbil is so transparent that the shape of this layer of ink, a perfect replica of the external TM surface, could be measured through the TM. We show in Figure 4 an example of a shape fringe map on a gerbil TM with our real-time moiré equipment.[21,24] This technique uses an image stored in an image memory and subtracts in real-time (25 times per second) the current image from a video camera. When the stored image corresponds to fringes projected on a flat object (a small coated plate) we obtain TM shape images; when we store a fringe image of the TM under zero pressure and then apply pressures to the membrane, we obtain real-time displacement fringe maps, where fringes represent iso-displacement lines (Fig. 4a). We used this technique
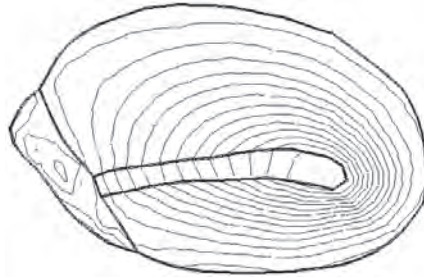
*Fig. 3.* Shape of the external surface of a cat TM shown as an image overlaid with contour lines of constant z, with an interval of 0.1 mm.



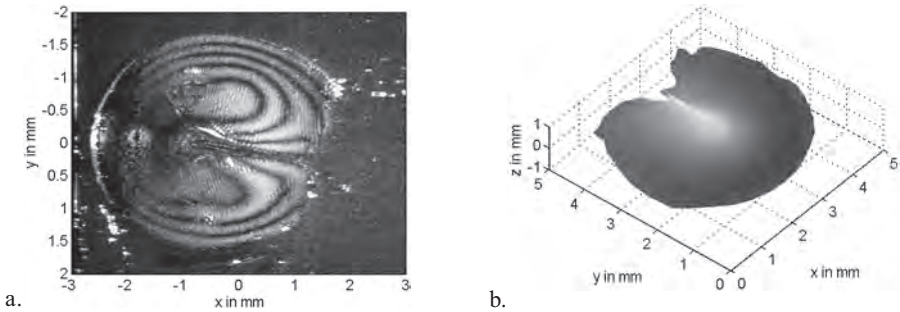a.                                                                    b.

*Fig. 4.* (a) Displacement map of a gerbil TM recorded with a real-time projection moiré set-up. The image of the medial surface of the TM is overlaid with moiré contours that represent iso-displacement lines with an inter-fringe interval of 0.108 mm. (b) Shape of the medial surface of a gerbil TM measured with a moiré-shift projection set-up. Grey level is used to encode the height coordinate *z*.

to study TM deformation for stepwise increasing static pressure loads in normal middle ears and in ears with known pathologies.[24-26]

The most recent version of moiré equipment in the Antwerp laboratory uses a projection moiré technique.[18,19] The requirement in shadow-moiré that the object be close to the grating is here relaxed. The fringe-shift technique is also implemented in such a way that the measurement directly provides a shape image matrix with high *x*, *y* and *z* resolutions. An example of a measurement performed with this setup, showing the shape of the medial surface of the pars tensa of a gerbil TM, with the T-beam-shaped manubrium seen on top, is given in Figure 4b.

Microscopic X-ray computed tomography

More recently, we have also measured the shape of the lateral TM surface in human, cat and gerbil using microscopic X-ray computed tomography (μ-CT). With μ-CT, 3-D models of the middle-ear structures can be made based on a set of virtual cross-sections.[27] The extremely thin soft tissue of the TM in ger-

bil and cat is hardly visible on μ-CT scans, but after applying some white draw-
ing ink through the ear canal onto the TM, the ink layer shows up on the scans
and can be used to measure the TM surface topography. (In humans, the TM
is considerably thicker and can be better discerned.) With this technique, the
entire TM can be measured from edge to edge, and when a scan of a pressur-
ized TM is also taken the functional boundary can easily be determined. The
μ-CT method demands a longer measuring time than the moiré method and re-
quires some tedious post-processing, mainly for the segmentation of the virtu-
al slice images. It has the advantage that other middle-ear structures can be
measured at the same time, but in contrast with the moiré method is not appli-
cable for real-time applications.

Magnetic-resonance imaging

Magnetic-resonance imaging is a scanning technique that is better suited to vi-
sualizing soft tissues with high water content than is X-ray CT. Magnetic-res-
onance microscopy (MRM) was introduced for use in the middle and inner ear
by the Hensons' group[28] and has been used successfully for creating middle-ear
models.[29] Unfortunately, MRM so far has a larger voxel size than μ-CT and
therefore direct imaging of the TM is sometimes marginal. Furthermore, MRM
does not provide good contrast between bone and air because neither has much
water content. To visualize the ossicles in the middle-ear air cavities, therefore,
it is necessary to fill the air cavities with a liquid contrast agent. This some-
times results in bubbles, and even in the absence of bubbles is likely to affect
the shape of the extremely flexible TM.[28]

*Derived geometrical parameters for the human tympanic membrane*

We have shown[22] that a lot of information can be extracted from a full-field TM
shape measurement such as that shown in Figure 2. We found, for example, that
the annulus (with a mean diameter on the order of 7 mm) is very close to pla-
nar; deviations out of the plane are mostly found in the superior posterior re-
gions and range over a small interval of ± 0.2 mm. The area of the TM surface
(surface area: pars tensa 62.1 mm$^2$, pars flaccida 3.3 mm$^2$) and of its projection
on the annulus plane (projected area: pars tensa 56.6 mm$^2$, pars flaccida 3.1
mm$^2$) can also easily be calculated.
    We also showed how the TM surface could be analyzed using, for example,
a series of cross-sections perpendicular or parallel to the manubrium. We pres-
ent here two such cross-sections, one through the umbo and perpendicular to
the manubrium in Figure 5a and one parallel to the manubrium in Figure 5b.
These sections illustrate very nicely the convex outward curvature of the TM.
It shows also that part of the TM covering the malleus handle is made up of two
almost rectilinear parts, one extending from the short process to about 4/5$^{th}$ of
the manubrium length, making an angle of 33° with the annulus plane, and the
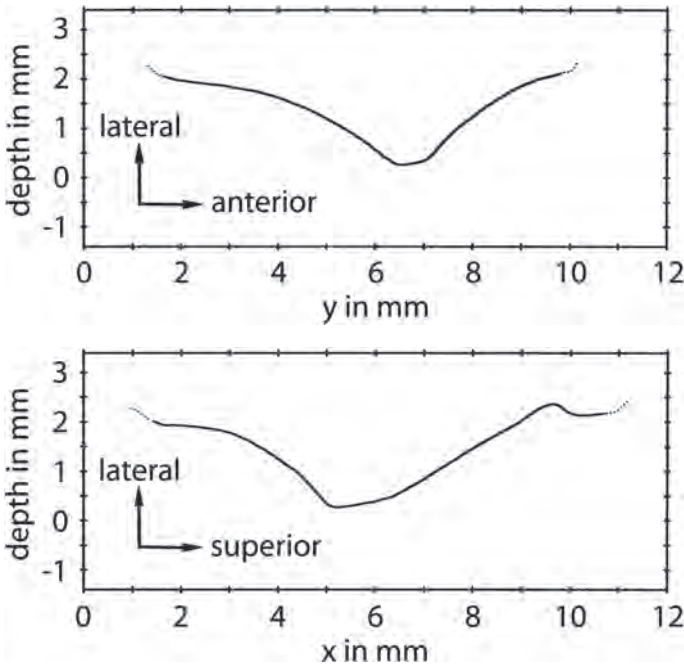
*Fig. 5.* (a) Cross-section of the human TM (data set of Fig. 2) in the direction perpendicular to the manubrium and going through the umbo. The TM's convex-outward curvature is prominent. Derived parameter such as cone depth can be read from the plot. (b) Cross-section of the human TM (data set of Fig. 2) along the manubrium. On this plot we can, for example, measure the angle between the TM surface covering the manubrium and the annulus plane.

remaining part extending inferiorly to the malleus tip, making an angle of 15° with that plane. The maximal depth of the TM cone was 1.74 mm below the annulus plane.

A very important application of the shape measurements is in formulating a highly realistic representation of the TM in a finite-element model. Figure 6 shows a 3-D view of a finite-element model for a cat TM. For this dataset the boundary of the annulus and manubrium was determined using static pressures as explained above.

## Human tympanic membrane cone depth and curvature during early development

In this section we present results of a small study on the morphogenesis of the human TM that was carried out years ago (1984) but never finalized as a paper. It fits nicely within the present context.

Six temporal bones with intact TM were used, with ages ranging from 12 fetal weeks to 11 years, plus three adult bones. The temporal bones were collected
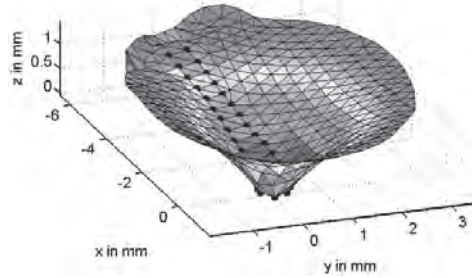
*Fig. 6.* Realistic finite-element model for a cat TM incorporating a representation for the TM based on a moiré shape measurement. The manubrium outline is emphasized with solid dots.

48 hours post mortem and stored in a solution of methanol. The ear canal was carefully dissected to completely expose the TM. An old version of our moiré interferometer, which still required fringe map analysis, was used to measure the 3-D TM shapes while the temporal bones were mounted with the annulus plane more or less parallel to the reference plane for the height contours (fringe planes). The fringe spacing was set at about 0.15 mm. The interferograms were used to trace cross-sections of the TMs perpendicular to the annulus plane, one perpendicular to the manubrium at the umbo (Fig. 7a), and one along the manubrium (Fig. 7b).

The border of the TM was estimated on the moiré contour maps, aided by direct observation of the temporal bones. The cross-sections in Figure 7 are limited to the external surface of the TM, excluding parts covered by overhanging bone.

Conclusions about the effects of age are limited by the small sample size, and by the effects of individual variations. (Optimally the same ear should be followed during its development; obviously this was not possible.) It is surprising that this 12-week fetal specimen has almost the size of the TM at birth. Between birth and the age of 11 years the size of the TM increases only slightly. The shape of the TM changes significantly. Between 12 fetal weeks and the age of six months the manubrium appears to rotate relative to the annulus. In reality it is the annulus that grows gradually from an almost horizontal position (with the superior edge tilted about 10° upward) to a more vertical position. As a result, the umbo gradually moves further below the annulus.[30]

To follow the depth of the TM cone as a function of age in samples collected from different ear, we have normalized the depth values (measured perpendicular to the line joining the ends of the curve) by dividing by the mean cross-section diameter of the sample (*i.e.*, the average of the widths of its cross-sections in Fig. 7a and 7b). The results are shown in Figure 8. The relative cone depth increases almost linearly with age in the first six months, to attain a value that is almost equal to that in the adult. The value for the adult TM shown on the graph is the mean of measurements on three adult temporal bones (0.294, 0.252 and 0.238 giving a mean of 0.26).

The curvature of the membrane is only indistinctly present at 12 fetal weeks
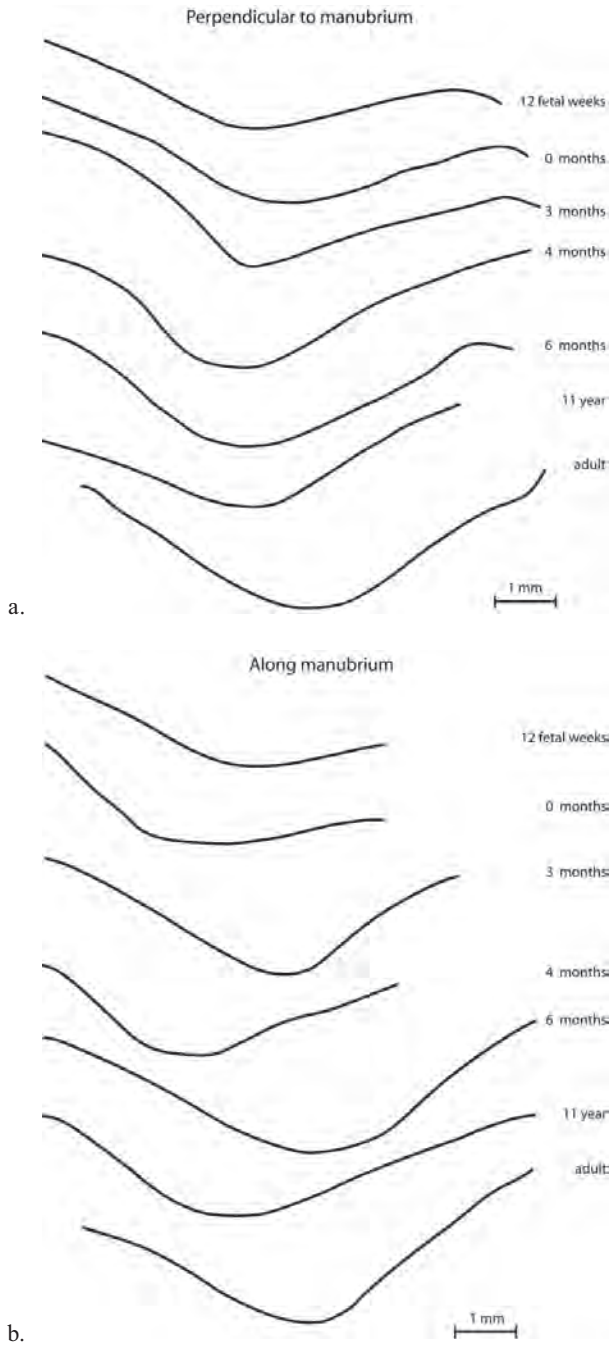
Perpendicular to manubrium

12 fetal weeks

0 months

3 months

4 months

6 months

11 year

adult

1 mm

a.

Along manubrium

12 fetal weeks

0 months

3 months

4 months

6 months

11 year

adult

1 mm

b.

*Fig. 7.* Development of cone depth and curvature illustrated with cross-sections perpendicular to the annulus for seven TM specimens of different ages. (a) Sections taken perpendicular to manubrium. (b) Sections taken along the manubrium at the level of the umbo. Specimen ages are given at the left of each curve.
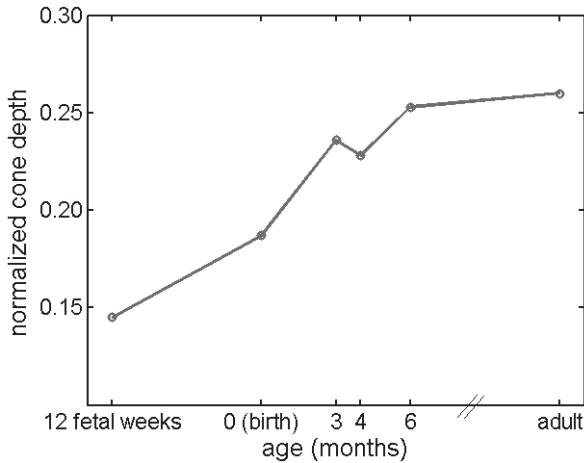
*Fig. 8.* Depth of the TM cone as a function of age. The measured depths were normalized for overall size by dividing by the mean cross-sectional diameter of the sample (average of the widths of its cross-sections in Fig. 7a and 7b). The relative cone depth increases almost linearly with age in the first six months. At six months the value is almost equal to that in the adult.

but is already pronounced at the age of three months. The curvature of the central part of the membrane is concave outward while the sides of the TM cone are convex outward. We hypothesized that the curvature of the TM is caused by a minimization of the elastic energy during this phase of its development.[31] The importance of the TM cone depth and of the curvature for TM function has been studied in papers by Funnell and Decraemer[23] and Fay *et al.*[32]

## Tympanic membrane thickness

In the 1980's, detailed data concerning TM thickness were sparse. Kojo[8] had measured the thickness at seven locations on each of seven human TMs: the total range was from 30 to 120 μm, with the average values for the seven locations ranging from 55 to 90 μm, the smallest values being in between the periphery and the manubrium. By comparison, Lim had reported that the human TM varies in thickness from 30 to 90 μm,[33] and that the cat TM is 30 to 50 μm thick and the guinea-pig TM is about 10 μm thick.[34]

    In 1982 Funnell and Laszlo[1] summarized by stating that 'more detailed measurements are required on variations of over-all thickness across the surface of the TM, and also on the thickness of the constituent layers'. Progress has been made during the present review period.

*Tympanic membrane thickness measurements with conventional light and electron microscopy*

To measure the thickness of ultra thin, virtually transparent and extremely delicate soft tissue membranes such as the TM, there is still no readily accessible method or tool available at present. Since the start of our present review period thickness measurements have been reported in the literature for cat,[35] gerbil[3,36] and human.[37,38] The thickness was at best measured at a few points on the TM whose locations were not clearly specified so a detailed thickness distribution was not obtained. The measurements were performed with conventional light or electron microscopy on histological sections of the TM. These techniques require a pre-treatment of fixing and dehydration prior to the sectioning and are likely to induce tissue shrinkage.

We have designed a method to measure the thickness distribution of an untreated TM (*i.e.* without fixation and dehydration) making use of the optical sectioning ability of confocal laser microscopy.[39] Errors caused by tissue preparation and sectioning are thus avoided. By carefully measuring thickness along a set of lines crossing the entire membrane from edge to edge, we can draw thickness distribution maps for the entire TM. Such maps, previously unavailable, will be extremely valuable in refining models of TM function. In the following sections we present details of the new method and then summarize some of the results obtained so far.

*Recent tympanic membrane thickness measurements using confocal laser microscopy*

Measurements were performed on fresh TMs. The TM within its intact annulus was dissected out of the temporal bone after opening the middle-ear cavity and removing the bulla wall to fully expose the medial face of the TM. The malleus was cut at the neck, leaving the manubrium attached to the membrane. During surgery the medial surface was kept moist by applying a few droplets of phosphate-buffered saline. The only other treatment that the TM underwent was soaking for 30 minutes in a water solution of Van Giesen dye, to make the tissue fluorescent. During the hours-long measurement session the tissue was embedded in glycerin/PBS to avoid desiccation.

A conventional confocal scanning microscope (LSM 410 Invert, Zeiss) was used. The TM was flattened out, as seen in Figure 9, on a Petri dish with part of the bottom replaced by a standard microscope cover glass.

Axial fluorescence images were obtained, that is, images in a plane parallel to the optical axis, perpendicular to the TM's surface. An example is shown in Figure 10a. The images were recorded from annulus to annulus along several lines perpendicular to the manubrium, and along one line parallel to the manubrium from the umbo to the inferior annulus edge. (For exact line positions *see* Fig. 9.) Using a water-immersion objective lens (Zeiss C-Apochromat 40× with NA = 1.2 and a 230-μm working distance) we obtained 320-μm-wide axial images with a lateral resolution of 0.3 μm and an axial resolution of 0.8 μm. Complete sections were obtained by apposition of a series of about 20 consecutive
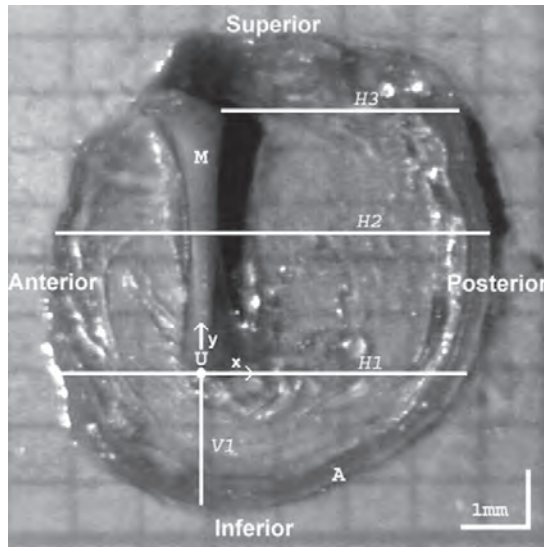
*Fig. 9.* Right cat TM flattened out on a supporting microscope slide, with its medial surface facing up ready for thickness measurement with the confocal microscope. A sheet of paper with a 1-mm grid is placed underneath to serve as a scale. Umbo (U), manubrium (M), annulus (A). Also indicated are the lines V1, H1, H2 and H3 where virtual sections were obtained. (Reproduced from [38]: JARO 6: 223-233 (2005) with permission from the Association for Research in Otolaryngology)

depth images. The position of each sub-image in the line and the distance between two lines (the $x$ and $y$ coordinates) were determined by two digital gauges with 1-µm accuracy. The umbo was chosen as the origin of a rectangular coordinate system and the specimen was oriented to have the $x$ axis perpendicular to the manubrium and the $y$ axis aligned along the manubrium in the superior direction (Fig. 9).

Thickness was determined on the cross-section of the TM, seen as a white band in the axial image (*e.g.,* Fig. 10a). In a small rectangular area about 20 µm wide (shown in Fig. 10a), the intensity of pixels at the same depth (in a horizontal direction on Fig. 10a) were averaged to obtain a smooth local intensity profile across the membrane (Fig. 10b). We showed that a good estimate of the membrane thickness is obtained as the width between points with half intensity values at the left and right 'shoulder' points (here at $z = \sim8$ µm and $z = \sim23$ µm) of the intensity plots, multiplied by a factor correcting for the mismatch in refractive index between the tissue and the mounting medium.[39] Thickness was calculated every 30 µm along entire scan lines.

Cat tympanic membrane thickness

The cat samples were harvested from euthanized cats and the thickness measurements performed a few hours post mortem. In Figure 11 we have plotted
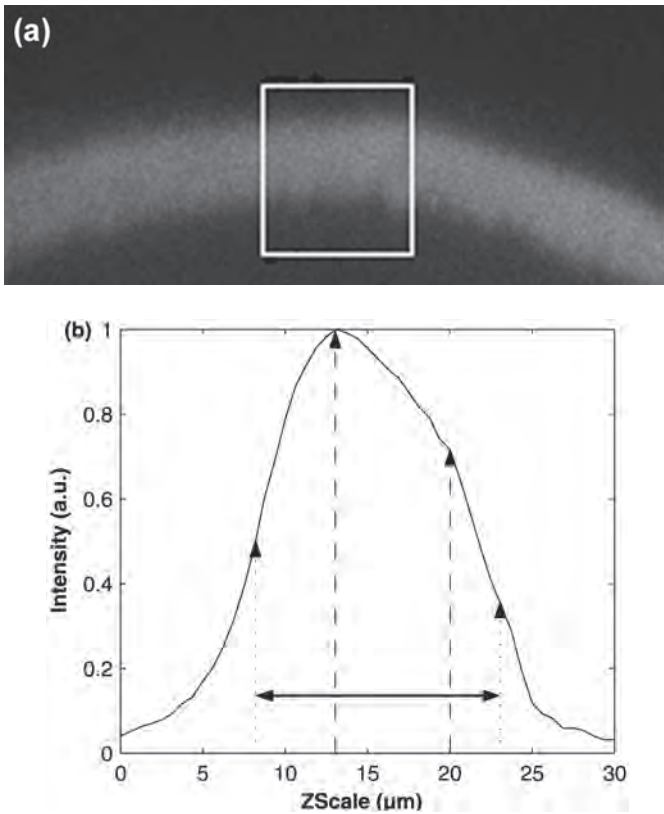
Fig. 10. (a) A small part of an axial image taken perpendicularly through the TM. The white, curved band is the TM cross-section, with the external surface upward. A selection (shown as a white rectangle) was taken through the cross-section and a laterally averaged intensity profile of the membrane in that section was obtained. (b) The averaged intensity profile of the cross-section of the tympanic membrane in the white rectangle shown in (a). Intensity is plotted as a function of the $z$-coordinate or depth. Dashed arrows: position of the 'shoulders' at the start and end of the slowly decreasing central part. Dotted arrows: position of the half-shoulder intensity. Horizontal arrow: thickness measure. (Reproduced from [38]: JARO 6: 223-233 (2005) with permission from the Association for Research in Otolaryngology)

thickness profiles for four left TMs: H1, H2 and H3 were scanned in the horizontal direction and V1 in the vertical direction as seen in Figure 9. We see that the different cats had surprisingly similarly TM thickness in all parts measured. The TM is also surprisingly thin for the larger part (about 12 µm) and thickens steeply and considerably (by a factor 4 to 5) when the annulus or the manubrium edge is approached.

Unfortunately, the measurements took too long for us to be able to measure thicknesses at a sufficiently dense matrix of points across the entire TM to permit automatic generation of its complete 2-D thickness map. Using all measured thickness data and assuming that thickness variations are gradual in both radial and circumferential directions, we manually constructed a thickness map by
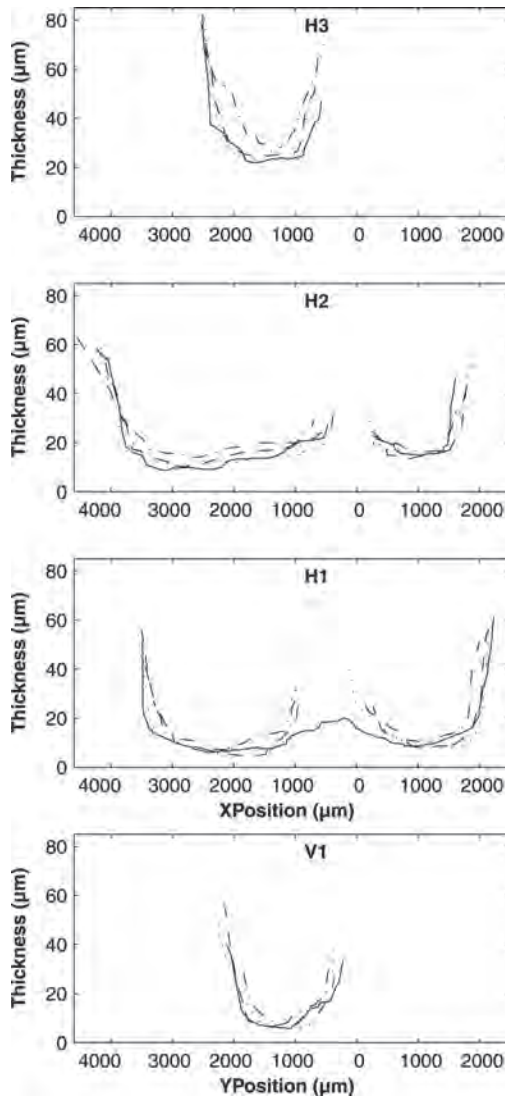
*Fig. 11.* Thickness as function of position along the H3, H2, H1 and V1 lines for four different left cat TMs. The solid line profile for H1 is taken somewhat more inferiorly than the other H1 profiles. Ant (anterior), Post (posterior), Inf (inferior), Sup (superior). (Reproduced from [38]: JARO 6: 223-233 (2005) with permission from the Association for Research in Otolaryngology)

2-D interpolation and extrapolation. Figure 12 shows this map as a contour plot. These data were taken from one right TM. The positions where data were actually measured (H1, H2, H3, V1) are also shown. Although we have measurements only along a few lines, the regularity and symmetry of the obtained contour plot makes us believe that the map shows a fairly good estimation of the real thickness.
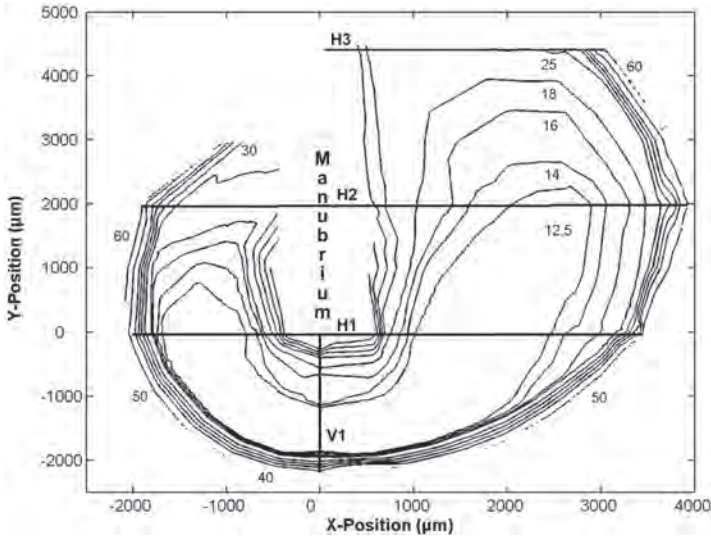
*Fig. 12.* Contour plot of the thickness distribution of a right cat TM. Thickness values are in micron (μm). The position of the manubrium, and the lines along which data were obtained, are indicated. (Reproduced from [38]: JARO 6: 223-233 (2005) with permission from the Association for Research in Otolaryngology)

The contour plot shows a gradual increase of thickness in the central area (*i.e.*, the area midway between the manubrium and the annulus) from the inferior (V1) region to the superior (H3) region, up to 25 μm anterior to the manubrium and 30 μm posterior to the manubrium. The TM is thinnest (about 12 μm) in the large inferior region encircling the lower part of the manubrium. The contour map is almost symmetrical with respect to the manubrium in the inferior region, growing more asymmetrical when moving superiorly: the posterior side is about twice as wide as the anterior side but only about half as thick as the anterior part at mid-manubrium height.

Lim[34] provides the only thickness values for cat in the literature, but does not explicitly specify the location where the histological sections were made. His value of 30 to 50 μm is three to four times as large as our minimal value and could be explained by a choice of samples relatively close to the annulus edge.

More information on our cat TM thickness measurements is presented in the paper by Kuypers *et al.*[40] Let us also mention that during our review period Chole and Kodama[35] published micrographs that allowed estimation of the cat TM thickness (and individual internal layer thickness). The thicknesses vary a lot within a given micrograph. The error of 10 μm given on the 40 μm TM thickness value in this paper is representative of this variation which was also seen and more clearly studied in the paper by Kuypers *et al.*[40]

Human  tympanic membrane thickness

In the present review period a few new thickness measurements on human TM became available, all based on measurements using conventional light microscopy. Uebo et al.[37] obtained mean thickness values between 50 μm and 150 μm for 10 regions in several TMs of humans of varying age. Schmidt and Hellström[41] measured thicknesses between 64 and 95 μm in a cross section through the umbo perpendicular to the manubrium at four points in the middle third of the anterior and the posterior parts. Ruah et al.[38] measured thicknesses in six different regions, with three measurement positions per region, for several TMs of humans aged between two days and 91 years. For adults, the following mean thicknesses were found: at the pars flaccida, 80 μm – 600 μm; at the pars tensa, posterosuperior 100 – 500 μm, posteroinferior 20 – 200 μm, anterosuperior 50 – 340 μm, anteroinferior: 30 – 430 μm; at the umbo 820 – 1700 μm.

Uebo et al. and Ruah et al. also studied the age dependence of TM thickness in human. Uebo et al. stated that for adults no significant change in thickness with age was observed. Ruah et al. found a thickness decrease in the posterosuperior zone and near the umbo from infants to adults, but later no relevant thickness changes were observed. The differences found between the age categories were not significantly larger than the differences found within categories. To summarize, it is clear that the data reported in the literature only cover small parts of the TM and show large differences.

With the confocal-microscopy technique described above and demonstrated for cat, we determined also the thickness of a human TM.[42] One human specimen that had been obtained in a fresh (untreated) condition was stored in physiologic solution and measured one day post mortem. Two other specimens were received preserved in a buffered formaldehyde solution. By applying the same preservation method to the fresh sample and re-measuring its thickness we could verify that the preservation method did not alter its thickness. Preparation for histological thickness measurement (decalcification, dehydrating, and sectioning) did significantly change the thickness; in the central region inferior to the umbo a shrinkage of up to 30% was observed. It therefore seems that TM thickness cannot be measured reliably from histological sections.

In Figure 13 we show a human TM thickness map, as was shown for cat in Figure 12. To avoid misinterpretation, we should emphasize that this one data sample is not representative of the absolute thickness of the human TM, as we observed large inter-individual differences. For the three TMs studied we found mean thickness values of 120, 50 and 40 μm. Combining this with the results found in the literature, we can state that there is no typical human TM thickness.

The relative thickness variation, on the contrary, was quite similar for all our samples. We found a large thin portion in the inferior region, extending in the posterior zone upward to mid manubrium, with a gradual thickening more superiorly. The anterior part was generally thicker than the posterior part: the thick-
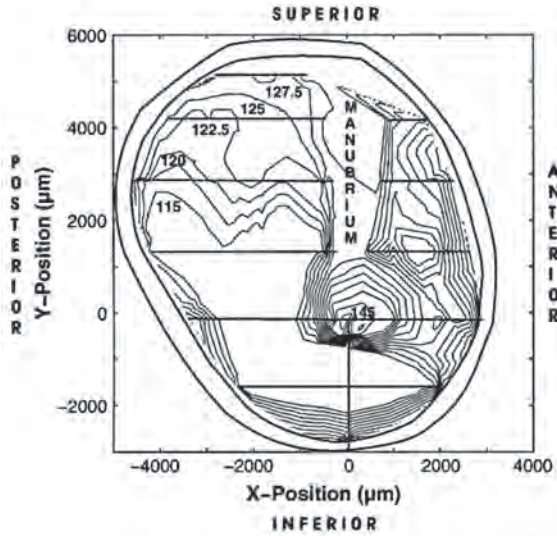
*Fig. 13.* Contour plot of the thickness distribution of an entire human left TM. Contours are shown for thicknesses between 115 and 145 μm, with a step of 2.5 μm. The positions of the scanning lines and the positions of the manubrium and annulus are indicated. (Reproduced from [40]: Otology and Neurotology 27: 256-264 (2006) with permission)

ness ratio was 1.06 to 1.31 μm for the H6 line (upper horizontal line in Fig. 13) and 1.02 to 1.83 for the H2 line (horizontal line crossing just below the umbo). Similar differences were also found by Kirikae et al.[9] (a ratio of 1.09) and Uebo et al.[37] (a ratio of 1.048) for the equivalent of our H2 line. As relative thickness distributions were similar for all measured membranes, one could use, for example, a thickness at the central part of a given membrane to rescale our sample distribution map to get a first-order estimate for the thickness of the entire TM. More data on our measurements of human TM thickness can be found in the paper by Kuypers et al.[42]

Gerbil  tympanic membrane thickness

The gerbil has become a widely used animal model in hearing research during this review period. So far, a homogeneous thickness has been assumed in all existing gerbil models. Based on histology, Teoh et al.[3] assumed a value of 19.1 ± 3.2 μm for the pars tensa and 32.2 ± 12.7 μm for the pars flaccida. Funnell et al.[43,44] and Ellaham et al.[45] used a gerbil pars tensa thickness of 5 μm and a pars flaccida thickness of 15 μm based on a histological study by von Unge,[36] who reported a thickness of 3-5 μm in the central region of the pars tensa between the annulus and the manubrium, a thickness of up to 20 μm near the annulus, and a thickness ranging between 10 and 20 μm for the pars flaccida.

We have determined TM thickness across the gerbil TM with our confocal laser scanning method.[46] We used healthy female gerbils (Meriones unguicula-

tus) with body weights of 67-119 g. Measurements were made for both the pars tensa and the pars flaccida. In gerbil the latter is much larger than in human and cat, and appears more like a separate entity than a part of the TM. The gerbil middle ear is much smaller than that in cat or human and is therefore very delicate and fragile. For this reason the TMs were not removed by dissecting them out at the annulus, but rather the thin bulla bone was removed around the annulus, leaving only a supporting ring of about 1 mm. The malleus was cut at the neck and the manubrium was kept in the membrane. The pars flaccida makes too large an angle with the pars tensa to make thickness measurements possible in a single preparation of both the pars tensa and pars flaccida. To measure pars flaccida thickness, the small circular membrane was cut out around its edge. Measurement locations on pars tensa and pars flaccida are illustrated in Figure 14.
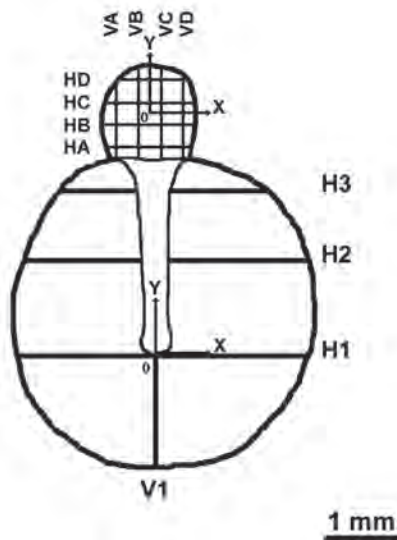


*Fig. 14.* A schematic representation of a gerbil TM. The coordinate system to describe the position of the pars tensa has the umbo as origin. The *x*-axis is oriented perpendicularly to the manubrium, pointing in the posterior direction. The *y*-axis is aligned along the manubrium, pointing in the superior direction. The imaged lines (V1, H1, H2, H3) are indicated. The coordinate system in the circular pars flaccida is positioned at the center. The orientations of the *x* and *y* axes are as for the pars tensa. The observation lines (VA, VB, VC, VD, HA, HB, HC and HD) form a grid with a step size of 300 μm and is positioned symmetrically around the origin. (Reproduced from [44]: Hearing Research 209 Vol. 1-2:42-52 (2005) with permission)

*Pars tensa*

Results of thickness measurements on the pars tensa of 11 gerbils are summarized in Figure 15. Interruptions of the thickness profiles are places were the manubrium is crossed. The uninterrupted H1 lines were measured slightly below the umbo, whereas the other H1 curves crossed the manubrium at the umbo.
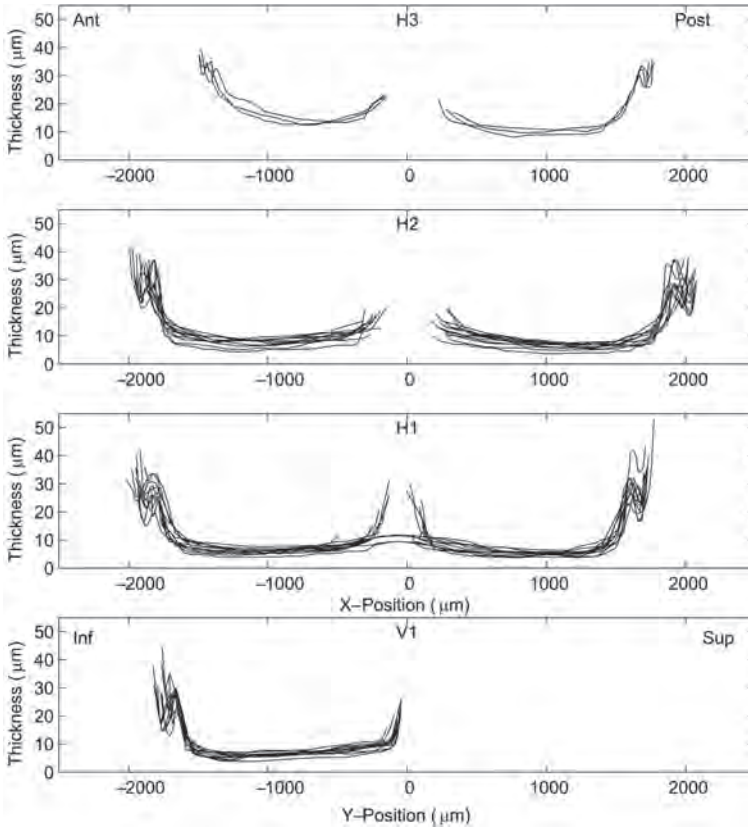


*Fig. 15.* Thickness as a function of position along the H2, H1 and V1 lines for 11 gerbil TMs (5 left and 6 right ears). The thickness scale has been expanded. The umbo was chosen as the origin for the *x-y* coordinate system. The thickness profiles that have a continuous H1 line in the region of the umbo ($x = 0$ µm) were measured along lines running slightly inferior to the umbo, while the interrupted H1 profiles crossed the umbo. Ant (anterior), Post (posterior), Inf (inferior), Sup (superior). (Reproduced from [44]: Hearing Research 209 Vol. 1-2:42-52 (2005) with permission)

In all panels of Figure 15, the thickness profiles from rim to manubrium are very similar for all animals measured. Thickness is smallest and rather constant in the central region between edge and manubrium. Thickness increases when approaching the peripheral rim. Close to the annulus the thickness decreases

again. There is thus a small bulge in the thickness profile which is seen all around
the outer edge; such a bulge was not seen in human or cat. Closest to the an-
nulus the membrane thickens steeply to a value about 5.5 times larger than the
thickness in the central region. When moving from the central region toward
the manubrium the thickness also increases. The thickness profiles for gerbil
are approximately symmetrical anterior and posterior to the manubrium. Along
all measured lines, the anterior side tends to be slightly thicker than the poste-
rior side. A gradual increase in thickness is also found when moving from the
most inferior part (V1) to the most superior part (H3). For all gerbils used, the
TM thickness was remarkably alike across individuals. In Table 1 we list val-
ues for the thickness in the thinnest central parts of the H1, H2, H3 and V1 lines
averaged over all animals tested. (Note that the H3 line was only measured in
three animals.)

| Thickness | Anterior | Posterior |
| --- | --- | --- |
| H3 | 14.38 ± 0.23 μm | 11.26 ± 0.21 μm |
| H2 | 8.00 ± 0.40 μm | 6.99 ± 0.27 μm |
| H1 | 6.42 ± 0.28 μm | 5.57 ± 0.22 μm |
| V1 | 6.34 ± 0.25 μm | |

The mean thickness in the thin central region was found to be between 5.6 and
14.4 μm. The mean thickness in the superior (H3) region is 2.3 times larger than
that in the inferior (V1) region in the anterior part, and 1.8 times larger in the
posterior part. Averaging the maximal thickness values near the annulus over
all lines gives 34.0 ± 0.7 μm.

   Interpolation, extrapolation and common sense were again used to construct
the thickness distribution map for the data of a right TM, shown in Figure 16.

   The near symmetry with respect to the manubrium found in the form and
shape of the gerbil TM is also found in the thickness map.

*Pars flaccida*

The lateral and medial surfaces of the pars flaccida are rugged, with abrupt thick-
ness variations of about 20%. To construct a meaningful thickness map we first
smoothed the thickness measurements along the different lines using a median
filter. We restrict the data shown here to a thickness map for one ear (Fig.
17).

   In the example shown we see that in the zone slightly above the center the
pars flaccida is thinnest, with an average thickness of 22 μm. In a second ger-
bil we found a value of 26 μm. The largest thicknesses were found at the edg-
es: when approaching the boundary between the pars flaccida and the pars
tensa, the thickness increases gradually over a large part of the radius to a fi-
nal value of about 200 μm; approaching the bony edge in the anterior, superi-
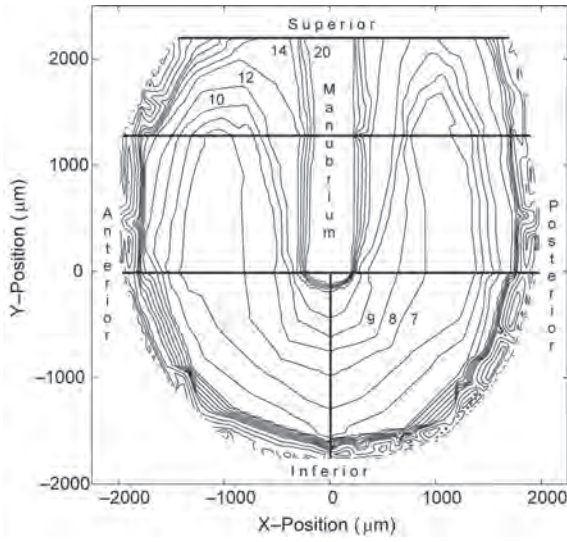
Fig. 16. Contour plot of the thickness of a right gerbil TM. Contours are plotted for thickness values of 7, 8, 9, 10, 12, 14, 16, 18, 20, 25, 30, 35 and 40 μm. The positions of the lines along which the data were obtained are indicated. (Reproduced from [44]: Hearing Research 209 Vol. 1-2:42-52 (2005) with permission)



Fig. 17. Contour plot of the thickness distribution of the pars flaccida of a left gerbil TM. Contours are plotted at thickness values between 22 and 70 μm with a step size of 4 μm. Some thickness values (in μm) are indicated at the corresponding contours. The positions of the scanning lines are also shown. (Reproduced from [44]: Hearing Research 209 Vol. 1-2:42-52 (2005) with permission)

or and posterior directions the thickness increases steeply over a distance of about a quarter radius to a final value of about 100 μm. (Note that in certain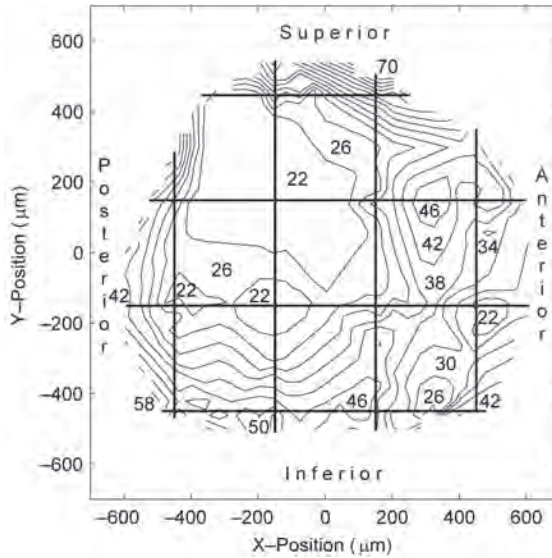 parts – here, for example, along the anterior edge – the very edge was missed during the difficult dissection of the very small pars flaccida.) The fine details of the thickness maps that we constructed for two different ears showed many differences, and the circular symmetry in the shape of the pars flaccida was not clearly repeated in the thickness map.

## Mechanical properties of the tympanic membrane

In the review by Funnell and Laszlo,[1] the following mechanical parameters of the TM were also discussed: elasticity (stiffness), Poisson's ratio, tension, internal damping and density. Based on that paper we first sketch the available observations of these parameters around 1980.

### *Stiffness*

Békésy[47] measured the bending stiffness of a human cadaver TM by cutting out a rectangular flap (2 mm × 0.5 mm) along three sides. He applied a known force (with a calibrated hair) to the free end and measured the displacement. Assuming the flap to be a uniform, isotropic cantilevered beam with a thickness of 50 μm, he used a standard formula from mechanics to calculate a Young's modulus of 20 MPa. (This modulus of elasticity describes the inherent stiffness of a material, and is defined as the ratio of a simple uniaxial stress applied to a material to the resulting strain parallel to the tension.) He stated that the value is about the same in the guinea pig, presumably on the basis of similar measurements.

Békésy[47] also measured the stiffness of the calf TM, using a somewhat different technique, and arrived at a Young's modulus that was smaller than the human one by a factor of $10^4$. This result is suspect because of the nature of the theoretical analysis used and because of the apparent abnormality of the TM studied.[48]

Kirikae[9] measured the stiffness of a strip (10 mm x 1.5 mm) of fresh human TM weighted at one end and suspended from a resonant cantilever rod at its upper end. From the system's resonance frequency (890 Hz) He calculated (again assuming uniformity and isotropy) a Young's modulus of 40 MPa with a formula containing the rod's resonant frequency (890 Hz), and the length and cross-section of the specimen, based on a TM thickness of 75 μm. (It appears that he actually used length and cross-sectional area values of 0.8 cm and $1.125 \times 10^{-3}$ $cm^2$ to obtain that result, rather than 1.0 cm and $1.25 \times 10^{-3}$ $cm^2$ as printed.) This value is twice that of Békésy's. Kirikae used a thickness of 75 μm. If he had used the thickness value of 50 μm as Békésy used, the computed modulus would have been higher. Kirikae reported that he obtained the same results when the

weight attached to the end of the TM strip was varied from 300 mg to 1000 mg, and interpreted it as an indication of material linearity.

Funnell and Laszlo[1] compared the Young's moduli measured in the TM with that of collagen. If one uses an effective thickness equal to that of the combined radial and circular layers (33 μm in Lim,[33] Fig. 4), instead of the total TM thickness, one should obtain a value for Young's modulus corresponding to the fibres themselves (assuming that they dominate the TM's mechanical properties, that the thickness is uniform, and that the combination of the two layers is isotropic). Using Lim's thickness of 33 μm (reducing the overall thickness by a factor of ⅔), Békésy's[47] data yield a modulus of 70 MPa. Reducing Kirikae's TM thickness by the same ratio would give 60 MPa. Using the thickness of either the radial or circular layer alone would raise the value further. It is interesting to compare this elasticity to values measured for other collagenous tissues. Haut & Little[49] found a stiffness of 100 to 200 MPa for an 'almost entirely collagenous' ligament when the strain was high enough that the fibres were being stretched rather than just re-oriented. Under similar conditions, Grahame[50] found a stiffness of 10 to 100 MPa for human skin in vivo (with considerable individual variation as well as dependence on age and sex). These figures are quite similar to the values measured for the TM. In 1980 there was some doubt as to whether the fibres in the TM were collagen [*e.g.*, ref. 51]. Recent work seems to indicate that the fibres do consist of collagen, of various types [*e.g.*, ref. 52]. In any case, their mechanical properties appear to be similar to those of collagen.

We ourselves have published data on TM viscoelasticity[53,54] and shall elaborate on these measurements in a separate section below.

*Poisson's ratio*

Poisson's ratio is the ratio of transverse to axial strain when a material is submitted to uni-axial stress. It has never been measured for the TM. For common materials it ranges from about 0.3, for isotropic crystalline solids, to 0.5 for incompressible rubber-like materials.[55] For a material composed of parallel fibres with no lateral interaction among the fibres, Poisson's ratio would be zero for a stress applied in the direction of the fibres. Since there were no experimental data to decide the issue, Funnell and Laszlo[1] proposed a value of 0.3 for the Poisson's ratio of the TM, but nowadays we think a value close to 0.5 is to be preferred, emphasizing incompressibility. The behaviour of the TM is probably not very sensitive to the value of Poisson's ratio.[29]

*Tension*

The only attempts that have been made to experimentally evaluate the degree of tension in the TM are those of Békésy[47] and Kirikae.[9] Békésy cut out U-shaped flaps in the TM. In the calf and sheep the flaps shrank and the cut-out hole ex-

panded, which he interpreted as evidence of tension. The shrinkage and expansion occurred over a period of about ten seconds, which Békésy interpreted as evidence for a large viscosity in the TM; it might also indicate that the shrinkage and expansion were a result of tissue drying or other effects along the cut edges, rather than tension release. In any case, the flaps apparently did not shrink in the human and guinea-pig TMs, since he stated that they were not under tension.

Kirikae investigated TM tension by cutting slits with a small paracentesis knife at various positions and orientations on human cadaver TMs, both with and without removing the epidermal layer. The only slits that became enlarged, suggesting tension, were those cut perpendicular to the radial fibres in TMs with the epidermis removed. Kirikae interpreted his results as confirming Békésy's finding that the internal tension of the TM, with the epidermis intact, is 'almost equal in every direction'. If the spreading of the slits really indicates tension, however, then Kirikae's observations also indicate that the radial fibres are under more tension than the circular ones, but that the epidermis is able to resist the tension. This would suggest that the epidermal layer is more significant mechanically than is generally assumed.

It is uncertain that tests such as the above are sensitive enough to detect tension in the TM. If one assumes that the resting tension in the TM is comparable to the tension that can be developed by the tensor tympani, then one can calculate that the amount of radial-fibre stretch to be released by a slit is on the order of 25 μm.[48] For a short slit the release would be less because of the restraints imposed by neighbouring fibres. An enlargement of a slit or flap by 25 μm would be difficult to detect, and might indeed be caused by local structural damage in the act of cutting.

The fact that Békésy's and Kirikae's experiments were done on cadaver ears obviously means that they could not detect any component of TM tension due to tonus in the tensor tympani. Also, any tension maintained passively by the ossicular ligaments might be sensitive to post-mortem tissue changes.

Helmholtz[56] believed that the curvature of the TM was maintained by a tension working against the circular fibres. That the curvature cannot all be explained as due to resting tension is indicated by the observation that a completely detached human TM, after being 'rolled up, [...] unfolds itself rapidly under water, and displays its exact contours' (Politzer, 1889, p. 76).[57]

The recent discovery of smooth muscle in the fibrocartilaginous ring [*e.g.*, ref. 58, 59] might suggest the existence of some tension in the TM, but at the moment we must say that there is no good evidence for resting tension in the TM.

*Internal damping*

Little attention has been paid to vibration damping in collagenous tissue. Witnauer & Palm[60] estimated the internal resistance of leather from the width of

the resonance in their measurement of the dynamic modulus of elasticity. The ratio of the modulus of elasticity to the internal resistance was found to be about $10^3$ sec$^{-1}$ at their observed resonance frequency of 15 to 20 Hz. Consistent with this, more recent measurements in strips of TM suggest that the internal damping is unimportant at least up to 300 Hz.[54]

*Density*

The TM probably has a more or less constant volume density, somewhere between that of water (1000 kg m$^{-3}$) and that of undehydrated collagen (1200 kg m$^{-3}$).[61] The epidermal, mucosal and loose connective-tissue layers are probably somewhat less dense than the fibrous layers.

The main conclusion of this section is probably that measurements of the mechanical parameters are sparse to non-existent. Apart from the elastic modulus, no significant studies on mechanical TM properties were made in the last few decades. Our discussion on recent observations is therefore restricted to the stiffness.

**Tympanic membrane elasticity**

In the distant past we made direct measurements of TM viscoelasticity. Parts of the work were published.[53,54] These papers were touched upon in Funnell and Laszlo's review;[1] in the following section we shall give further details, some of them previously unpublished. In the same section we discuss very recent measurements of human TM elasticity by Cheng *et al.*[62] Recently Fay *et al.*[63] estimated the elastic modulus of the TM using three different approaches; this is briefly discussed in the second part of the following section.

*Direct elasticity measurements*

Soft biological tissues show typical viscoelastic behaviour: the relation between stress and strain is time dependent. When, for example, a constant stress is suddenly applied to a sample in a unidirectional tensile test the strain will, after a sudden increase, gradually increase further with time ('creep'). The stress is also dependent on the history of deformations ('strain history') that a sample underwent prior to the present test. In a cyclic loading-unloading experiment, for example, the stress will depend on the number of previous cycles ('hysteresis loop'). As successive loading and unloading experiments tend to a steady state ('preconditioning'), and as the hysteresis loops corresponding to strongly different strain rates (varying by up to a factor of $10^3$) do not depend much on the strain rate, we find in the literature many attempts to describe ascending and/or descending branches of a loading-unloading curve by a purely elastic stress-strain relation. We shall first discuss TM elasticity using this approach.
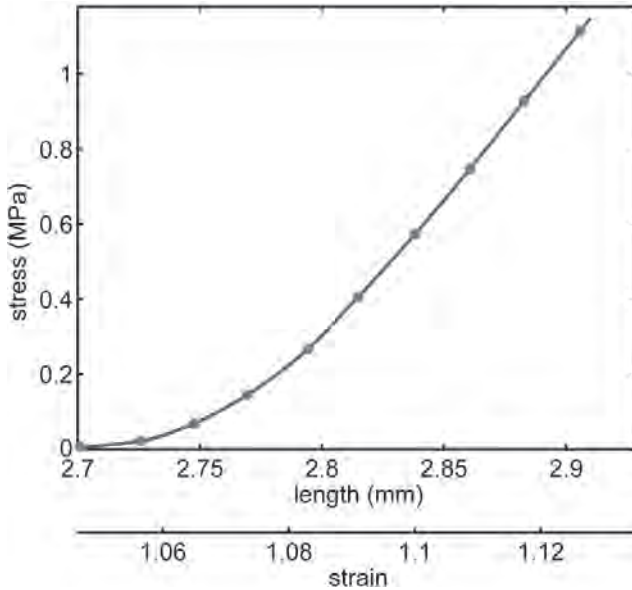
*Fig. 18*. Stress-length relation for a strip of fresh human TM recorded during a tensile-test experiment. Only the loading branch is shown: slow onset at smallest strain, strong non-linear middle part and linear end portion. Based on the entire curve the rest-length $l_0$ was estimated and the strain $l/l_0$ was then calculated. Strain is shown on the second abscissa underneath the length axis. The Young's modulus calculated from the slope of the quasi-linear end part of this curve is 22 MPa. (This figure shows the same data as Fig. 3 in [52]. We discovered while writing this review that the scale factor for the abscissa in that paper should have been $10^6$ N/m$^2$ (or $10^6$ Pa) and not $10^7$ N/m$^2$ as originally published. Parameter values in the annotation were correct.)

Let us, as an example, consider in Figure 18 the loading branch of a stress-length relation for fresh human TM obtained when a thin strip of tissue was subjected to a uniaxial tensile test after preconditioning was reached.

We deliberately did not at first use strain on the abscissa because that requires knowledge of the resting length of a specimen: the slope of the stress-strain curve starts at zero and increases so slowly with increasing extension of the sample that it is practically impossible to pick out the point – the rest length – where the stress suddenly starts to deviate from zero. In the paper by Decraemer *et al*.[53] we proposed a non-linear elastic structural model for biological tissue and based upon it a procedure for estimating the rest length using the entire stress-length curve. Afterward the stress-length curve can be expressed as a stress-strain curve. The strain on the lowermost abscissa of Figure 18 was calculated by means of this rest-length estimate.

Even when we do ignore the fact that the loading and unloading branches of a stress-strain relation are different, the non-linear stress-strain curve illustrates the difficulty with a soft biological tissue of specifying its stiffness by a single number, and the difficulty in comparing such numbers from different sources

in the literature.

When large deformations are considered, it is obvious from Figure 18 that the stress cannot be calculated simply as stiffness times strain. As a first approximation we can use a constitutive equation based on a structural model, or a purely phenomenological stress-strain fitting function containing parameters without direct physical meaning.

When one tries to model large deformations of a real 3-D structure, such as the TM under a static pressure load, geometric non-linearities are also encountered, making the modelling even more complex. Displacements may indeed be so large that the influence of changing geometry must be taken into account. Ladak *et al.*[64] modelled such TM displacements using a single value for the elastic modulus and including only geometric non-linearity in a model. Results showed the importance of the geometrical non-linearity but did not rule out the importance of material non-linearity, at least under some conditions.

When small acoustical vibrations are considered we can as a first approximation estimate a working point on the stress-strain curve and determine an incremental stiffness as the slope of the stress-strain curve at the working point. The approximation, for both large and small deformations, obviously neglects all viscous effects. When in a uniaxial tensile test, for example, small sinusoidal length changes are applied to a pre-loaded specimen, small loops are recorded when stress is plotted as a function of strain. For sufficiently small deformations, the stress is approximately sinusoidal and the loop can be described by an amplitude ratio of stress and strain (the incremental elastic modulus) and a small phase angle between stress and strain (about $5°$ for the TM, and quite independent of frequency[54]). Mathematical modelling of the middle ear is usually done for acoustical stimuli and the value of the stiffness used in the model can be considered as an incremental modulus. To account for phase differences an extra damping (internal viscosity) parameter has to be included in the model. Unfortunately, to choose an incremental modulus we need a good estimate of the working point on the stress-strain curve in a normal physiological situation or during experiments on temporal bones or anesthetized animals. The difficulty of estimating the tension in the TM was discussed above.

Most viscoelastic constitutive equations were originally introduced for engineering applications with non-biological materials and are not perfectly suited for use with soft biological tissue. In a study on viscoelasticity we have proposed a non-linear viscoelastic constitutive equation for soft biological tissues[54] and used it to describe experimental data from dynamic measurements (unidirectional tensile test with small sinusoidal deformations superimposed on a pre-strain) on three small rectangular samples cut out from fresh human TMs (length 3 to 5 mm, width 2 to 4 mm, thickness 0.07 to 0.1 mm). Values obtained for the incremental elastic modulus, normalized for a constant pre-strain level of 0.15 and a superimposed sinusoidal strain with amplitude of 0.01, were 17.4, 25.8 and 16.4 MPa, for an average value of 20 MPa. The pre-strain level was calculated based on the rest-length estimate based on a loading-unloading ex-

periment on the same specimen, as explained above, and situates the working point on the quasi-linear portion of the stress-strain curve for large strains. This value for the elastic modulus is significant because it is valid over a relatively large range of strains, but let us emphasize that this range was not chosen on the basis of a known physiological pre-strain level. Our average dynamic (incremental) elastic modulus compares well with the static values obtained by Békésy,[47] and Kirikae[9] (as described above), in spite of the different experimental methods used.

Very recently new experimental observations of the Young's modulus of human TM were published by Cheng et al.[62] Small strips cut from the posterior part of the TM, parallel to the manubrium (lengths 5 to 8.5 mm and widths 1.5 to 2.5 mm), were studied in quasi-static unidirectional elongation tests with a method very similar to that of Decraemer et al.[53] The stress-strain curves of Cheng et al. are quite similar to the ones obtained by Decraemer et al. Graphs of the Young's modulus as a function of stress and strain are shown. At their maximum strain of 1.13, a Young's modulus of 18 MPa was found, which is in good agreement with the value of 22 MPa for a strain of 1.12 obtained by Decraemer et al. Preliminary stress-relaxation tests were also presented by Cheng et al. reflecting the viscoelastic character of the TM, consistent with that demonstrated by Decraemer et al. in their study on TM viscoelasticity.[54]

*Indirect elastic modulus estimates*

A completely different way of estimating the elastic modulus of the TM was adopted by Fay et al.[63] Three different approaches are used. First, constitutive modelling is used to estimate an elastic modulus based on the elastic modulus of collagen and on experimentally observed fibre densities in the TM. Second, experimental tension and bending test results from the literature are re-interpreted using composite laminate theory. Last, measurements of vibrations of the cat TM are used in conjunction with a composite shell model to determine upper and lower limits for the material parameters. For humans the data suggest a range for the elastic modulus between 100 and 300 MPa. For cat the data suggest a range of 100 to 400 MPa. For human, these values are about 4 to 10 times larger than the previous estimates discussed above.

For cats there are no direct measurements in the literature for comparison, but these values are also 4 to 17 times larger than the Young's modulus used in cat TM finite-element models that seem to match experimental vibration amplitude and frequency data fairly well.[65,66] At least part of the discrepancy between the Young's moduli of Fay et al. and the earlier ones is explained by the fact that Fay et al. used thicknesses corresponding to just the radial and circular fibre layers rather than the overall TM thickness. Furthermore, one of their approaches to estimating the Young's modulus of the TM is based on observations of acoustic vibrations of the TM over a wide frequency range (100 Hz – 22 kHz). To fit these dynamic observations it is not surprising that Young's

moduli higher than the values from static tests are required: Decraemer *et al.*[54] found that on a log-log plot the Young's modulus increases linearly with frequency in the 0.01-to-100 Hz range.

## Conclusion

In this chapter we started with outlining what was known about anatomical and mechanical parameters of the TM around 1980, based on a review paper by Funnell and Laszlo. We then discussed new data that became available in the present review period, 1980-2007. Unfortunately we must conclude that to date good data for many of the mechanical properties of the TM, whether directly measured or indirectly estimated, are still lacking.

## Acknowledgements

## References

1. Funnell WRJ, Laszlo CA. A critical review of experimental observations on eardrum structure and function. *ORL* 1982; 44: 181-205. [Starting with the earliest observations, it sketches the history of eardrum properties till about 1980.]
2. Todd NW. Orientation of the manubrium mallei: inexplicably widely variable. Laryngoscope 2005; 115: 1548-1552.
3. Teoh SW, Flandermeyer DT, Rosowski JJ. Effects of pars flaccida on sound conduction in ears of Mongolian gerbil: acoustic and anatomical measurements. Hearing Research 1997; 106: 39-65.
4. Dirckx JJJ, Decraemer WF, von Unge M, Larsson C. Volume displacement of the gerbil eardrum pars flaccida as a function of middle ear pressure. Hearing Research 1998; 118: 35-45.
5. Hellström S, Stenfors L-E. The pressure equilibrating function of pars flaccida in middle ear mechanics. Acta Physiol Scand 1983; 118: 337-341.
6. Didyk LA, Dirckx JJJ, Bogdanov VB, Lysenco VA, Gorgo YP. The mechanical reaction of the pars flaccida of the eardrum to rapid air pressure oscillations modeling different levels of atmospheric disturbances. Hearing Research 2007; 223: 20-28.
7. Fumagalli Z. Morphological research on the sound-transmission apparatus. Arch Ital Otol Rinol Laringol 1949; 60: Suppl. 1, ix + 323 pp. [In Italian, captions & chapter 7 in English also]
8. Kojo Y. Morphological studies of the human tympanic membrane. J ORL Soc Japan 1954; 57: 115-126. [In Japanese]
9. Kirikae I. The structure and function of the middle ear. Tokyo: University of Tokyo Press 1960. pp. 36-59.
10. Khanna SM, Tonndorf J. Tympanic membrane shape determined by moiré topography. J Acoust Soc Am 1975a; 57: S72 (abstract).
11. Khanna SM, Tonndorf J: Tympanic membrane: effect of dc pressure changes in the middle ear of cats. J Acoust Soc Am 1975b; 58: S88 (abstract).

12. Funnell WRJ. Image processing applied to the interactive analysis of interferometric fring-es. Applied Optics 1981; 18: 3245-3249.

13. Decraemer WF, Khanna WF, Dirckx JJJ. The integration of detailed 3-dimensional anatomical data for the quantitative description of 3-dimensional vibration of a biological structure. An illustration from the middle ear. In: Tomasini EP (ed.) Vibration Measurements by Laser Techniques: Advances and Applications. SPIE 2002; 4827:148-158.

14. Dirckx JJJ, Decraemer WF. (1989). Phase shift moiré apparatus for automatic 3-D surface measurement. Review Scientific Instruments 1989; 60: 3698-3701. [New non-contacting technique opened door to measure eardrum shape in detail.]

15. Dirckx JJJ, Decraemer WF. Optoelectronic moiré projector for real-time shape and deformation studies of the tympanic membrane. J Biomed Optics 1997; 2: 176-185.

16. Dirckx JJJ, Decraemer WF. Video-moiré topography for in-vitro studies of the eardrum. In: Foth HJ, Marchesini R, Podbielska H (eds.) Optical and imaging techniques for biomonitoring III. Proceedings of Progress in Biomedical Optics, Europto Series. San Remo: Italy 1997. SPIE 3196: 2-11.

17. Dirckx JJJ, Decraemer WF, von Unge M, Larsson C. Volume displacement of the gerbil eardrum pars flaccida as a function of middle ear pressure. Hearing Research 1998; 118: 35-45.

18. Dirckx JJJ, Decraemer WF. Projection moiré interferometer for research in otology. In: Dalfante M, Foth HJ, Krasner H, Marchesini R, Podbielska H (eds.) Optical and Imaging techniques for Biomonitoring IV. Remo, Italy 1998. SPIE 3567: 120-129.

19. Dirckx JJJ, Decraemer WF. Interferometer for eardrum shape measurements, based on projection of straight line rulings. Lasers Med Sci 2000; 15: 131-139.

20. Dirckx JJJ, Decraemer WF. Moiré topography for basic and clinical hearing research. Recent Res Devel Optics 2003; 3: 271-296.

21. Dirckx JJJ, Decraemer WF. Real-time moire topography. In: Walker CA (ed.) Handbook of moiré measurements. Series in Optics and Optoelectronics, Institute of Physics Publishing 2004. Chapter 12.1, pp. 287-396.

22. Decraemer WF, Dirckx JJJ, Funnell WRJ. Shape and derived geometrical parameters of the adult, human tympanic membrane measured with a phase-shift moire interferometer. Hearing Research 1991; 51: 107-122. [First precise measurements of the shape of the entire eardrum.]

23. Funnell WRJ, Decraemer WF. On the incorporation of moiré shape measurements in finite-element models of the cat eardrum. J Acoust Soc Am 1996; 100: 925-932. [First incorporation of precisely measured eardrum shape in a mathematical model.]

24. von Unge M, Decraemer WF, Bagger-Sjöback D, J.J. Dirckx JJJ. Displacement of the gerbil tympanic membrane under static pressure variations measured with a real-time differential moiré interferometer. Hearing Research 1993; 70: 229-242.

25. von Unge M, Decraemer WF, Dirckx JJJ, Bagger-Sjöback D. Shape and displacement patterns of the gerbil tympanic membrane in experimental otitis media with effusion. Hearing Research 1995; 82: 184-196.

26. von Unge M, Decraemer WF, Bagger-Sjöback D. Tympanic membrane changes in experimental purulent otitis media. Hearing Research 1997; 106: 123-136.

27. Decraemer WF, Dirckx JJJ, Funnell WRJ. Three-dimensional modeling of the middle-ear ossicular chain using a commercial high-resolution x-ray CT scanner. JARO 2003; 4: 250-263. [Paper shows how well computer-aided imaging techniques are suited for applications to the middle ear.]

28. Henson MM, Henson OW Jr, Gewalt SL, Wilson JL, Johnson GA. Imaging the cochlea by magnetic resonance microscopy. *Hearing Res* 1994; 75: 75-80.

29. Elkhouri N, Liu H & Funnell WRJ. Low-frequency finite-element modelling of the gerbil middle ear. JARO 2006; 7: 399-411.

30. Ars B, Ars-Piret N. Dynamics of the organogenesis of the middle ear structures. In: Ars B, Van Cauwenberge P (eds.) Middle ear structures and congenital defects. The Hague: Kugler Publications 1991. pp. 11-25.

31. Decraemer WF, Dirckx JJJ, Funnell WRJ, Ladak HM. The shape of the eardrum in cat closely resembles a minimal-surface spanning the handle of the malleus and the annulus. Abstract. Proceedings of the 23nd Midwinter Research Meeting of the Association for Research in Otolaryngology 2000, abstract 408.
32. Fay JP, Puria S, Steele CR. The discordant eardrum. Proc Natl Acad Sci (USA) 2006: 103: 19743-19748.
33. Lim DJ. Human tympanic membrane. An ultrastructural observation. Acta Otolaryngol 1970; **70**: 176-186.
34. Lim DJ. Tympanic membrane. Electron microscopic observations. Part I. Pars tensa. Acta Otolaryngol 1968; 66: 181-198.
35. Chole RA, Kodama K. Comparative histology of the tympanic membrane and its relationship to cholesteatoma. Annals of Otology, Rhinology, and Laryngology 1989; 98: 761-766.
36. von Unge M, Borg E, Bagger-Sjöback. The mechano-acoustic properties of the tympanic membrane: a study on isolated Mogolian gerbil temporal bones. Am J Otolog 1991; 12: 407-419.
37. Uebo K, Kodama A, Oka Y, Ishii T. Thickness of normal human tympanic membrane. Ear Res Jpn 1988: 19: 70-73.
38. Ruah CB et al. Age-related morphologic changes in the human tympanic membrane. Arch Otolaryngol Head and Neck Surg 1991; 117: 627-634.
39. Kuypers L, Decraemer WF, Dirckx JJJ, Timmermans JP. A procedure to determine the correct thickness of an object with confocal microscopy in case of refractive index mismatch. Journal of Microscopy 2005; 218: 68-78.
40. Kuypers LC, Dirckx JJJ, W.F. Decraemer WF, Timmermans JP. Thickness distribution of fresh eardrums of cat obtained with confocal microscopy. JARO 2005; 6: 223-233. [Most complete cat eardrum thickness map.]
41. Schmidt SH, Helstrom S. Tympanic membrane structure – new views. A comparative study. ORL Journal for Oto-rhino-laryngology and its Related Specialties 1991; 53: 32-36.
42. Kuypers LC, Decraemer WF, Dirckx JJJ. Thickness distribution of fresh and preserved human eardrums measured with confocal microscopy, Otology and Neurotology 2006; 27: 256-264. [Most complete human eardrum thickness map.]
43. Funnell WRJ, Decraemer WF, von Unge M & Dirckx JJJ. Finite-element modelling of the gerbil eardrum and middle ear. Abstract of the 22nd Midwinter Meeting of the Association for Research in Otolaryngology, St. Petersburg Beach, FL 1999.
44. Funnell WRJ, Decraemer WF, von Unge M & Dirckx JJJ. Finite-element modelling of the gerbil eardrum and middle ear. Abstract of the 23rd Midwinter Meeting of the Association for Research in Otolaryngology, St. Petersburg Beach, FL 2000.
45. Ellaham NN, Akache F, Funnell WRJ, Daniel SJ. Spatial vibration patterns of the gerbil eardrum. *Can Acoustics* 2007; 35: 72-73.
46. Kuypers LC, Dirckx JJJ, Decraemer WF, Timmermans JP. Thickness of the gerbil tympanic membrane measured with confocal microscopy. Hearing Research 2005; 209: 42-52. [Most complete gerbil eardrum thickness map.]
47 Békésy G. Experiments in Hearing. Toronto: McGraw-Hill 1960.
48. Funnell WRJ. A theoretical study of eardrum vibrations using the finite-element method. PhD. thesis (McGill University, Montréal 1975, updated 1976)
49. Haut RC, Little RW. The rheological properties of canine anterior cruciate ligaments. J Biomech 1969; 2: 289-298.
50. Grahame R. A method for measuring human skin elasticity *in vivo* with observations on the effects of age, sex and pregnancy. Clin Sci 1970; 39: 223-238.
51. Johnson, FR; McMinn, RMH, & Atfield, GN. Ultrastructural and biochemical observations on the tympanic membrane. J Anat 1968; 103: 297-310.
52. Stenfeldt K, Johansson C & Hellström S. The collagen structure of the tympanic membrane.

Collagen types I, II, and III in the healthy tympanic membrane, during healing of a perfora-
tion, and during infection. Arch Otolaryngol Head Neck Surg 2006; 132: 293-298.

53. Decraemer WF, Maes MA, Vanhuyse VJ. An elastic stress-strain relation for soft biological tis-
sues based on a structural model. J. Biomechanics 1980; 13: 463-468.

54. Decraemer WF, Maes MA, Vanhuyse VJ, Vanpeperstraete P. A non-linear viscoelastic consti-
tutive equation for soft biological tissues, based upon a structural model. J Biomechanics 1980;
13: 559-564.

55. Snowdon JC. Vibration and shock in damped mechanical systems. New York, NY: Wiley
1968.

56. Helmholtz HLF. The mechanism of the middle-ear ossicles and of the eardrum. Pflüaut;gers
Arch. f. Physiol. (Bonn) 1: 1-60 [in German] (1869) [transl. by Buck, AH, & Smith, N (New
York: Wood & Co. 1873) and by Hinton J, Publ. New Sydenham Soc. (London) 62: 97-155
(1874)]

57. Politzer A. The anatomical and histological dissection of the human ear in the normal and
diseased condition (Stuttgart: Enke 1889) [In German, transl. by Stone G (Baillière, Tindall
& Cox, Strand 1892)]

58. Henson OW Jr, Henson MM. The tympanic membrane: highly developed smooth muscle ar-
rays in the annulus fibrosus of mustached bats. J Assoc Res Otolaryngol 2000 1; 25-32.

59. Yang X, Henson OW Jr. Smooth muscle in the annulus fibrosus of the tympanic membrane:
physiological effects on sound transmission in the gerbil. Hearing Res 2002; 164: 105-114.

60. Witnauer LP, Palm WE. Preliminary studies of dynamic mechanical properties of leather. Am
Leather Chemists Ass J 1961; 56: 58-67.

61. Harkness RD. Biological functions of collagen. Biol Rev Cambridge Phil Soc 1961; 36: 399-
463.

62. Cheng T, Dai C, Gan RZ. Viscoelastic properties of human tympanic membrane. Ann Biomed
Eng 2007; 35: 305-314.

63. Fay J, Puria S, Decraemer WF, Steele C. Three approaches for estimating the elastic modu-
lus of the tympanic membrane. J Biomechanics 2005; 38: 1807-1815.

64. Ladak H, Funnell WRJ, Decraemer WF, Dirckx JJJ. A geometrically nonlinear finite-element
model of the cat eardrum, J Acoust Soc Am 2006; 119: 2859-2686.

65. Funnell WRJ, Decraemer WF & Khanna SM. On the damped frequency response of a finite-
element model of the cat eardrum. *J Acoust Soc Am* 1987; 81: 1851-1859.

66. Funnell WRJ, Decraemer WFS & Khanna SM. Damped vibration patterns on a finite-ele-
ment model of the cat eardrum. Abstr. 22nd Midwinter Meeting of the Association for Re-
search in Otolaryngology, St. Petersburg Beach, FL 1997.